Journal of Materials Chemistry A

COMMUNICATION

View Article Online
View Journal | View Issue

Published on 14 September 2015. Downloaded by University of Washington on 19/05/2016 10:25:42.

Cite this: J. Mater. Chem. A, 2015, 3, 20103

Received 12th August 2015
Accepted 10th September 2015

DOI: 10.1039/c5ta06339f

www.rsc.org/MaterialsA

Impact of lithium excess on the structural and electrochemical properties of the $LiNi_{0.5}Mn_{1.5}O_4$ high-voltage cathode material†

Yu-Feng Deng,[ab] Shi-Xi Zhao,*[ab] Peng-Yuan Zhai,[ab] Guozhong Cao[c] and Ce-Wen Nan[b]

$LiNi_{0.5}Mn_{1.5}O_4$-based cathode materials are synthesized by a one-step nonaqueous co-precipitation method. Appropriate excess lithium ions can extrude transition metal ions out of tetrahedral 8a sites, which could have a higher effect on the rate performance of $LiNi_{0.5}Mn_{1.5}O_4$ than the well-known factor, *i.e.* cationic order degree in 16d octahedral sites.

$LiNi_{0.5}Mn_{1.5}O_4$ is a promising cathode material for lithium-ion batteries as it offers a high operating voltage of ~4.7 V arising from the $Ni^{2+/4+}$ couple instead of the $Mn^{3+/4+}$ couple of spinel $LiMn_2O_4$.[1,2] It possesses two similar crystal structures. One with a random distribution of Mn^{4+} and Ni^{2+} ions in the octahedral 16d sites displays the disordered phase with the space group of $Fd\bar{3}m$. Another belongs to the space group of $P4_332$ with an order arrangement of Mn^{4+} and Ni^{2+}. The real structure of $LiNi_{0.5}Mn_{1.5}O_4$ contains both phases.[3] Factors influencing the performance of $LiNi_{0.5}Mn_{1.5}O_4$ mainly reported are cationic order degree in octahedral 16d sites[4,5] and surface planes.[6,7] Generally the material with a lower cationic order degree is thought to have better rate performance because of its higher Li-ion diffusion coefficient.[8]

Changing annealing conditions[9] is a traditional way to control the cationic order because Mn^{3+} derived from oxygen vacancies hinders this order degree. Whittingham *et al.*[10] prepared disordered $LiNi_{0.5}Mn_{1.5}O_4$ with high-rate capability by increasing Mn^{3+} concentration. Meanwhile some other methods such as varying the Ni/Mn ratio,[11] doping[12] and the polymer-assisted method[13] also could be actualized to control the cationic order with no need for further annealing. However a common phenomenon, namely some amount of transition metal ions (Ni^{2+} and/or Mn^{4+}) occupy the tetrahedral 8a sites instead of original Li^+ ions, which usually is overlooked. Means applied to control the cationic order degree in octahedral 16d sites could even enhance this staggered arrangement.[14–18] Though the mixing effect between lithium ions and transition ions in cathodes materials with a layered structure has been proven to be unfavorable to rate ability,[19] its effect on the performance of spinel $LiNi_{0.5}Mn_{1.5}O_4$ has not received enough attention.

In an attempt to clarify the role of tetrahedral 8a site occupation, a simple method was carried out: appropriate excess lithium ions can extrude transition ions out of tetrahedral 8a sites without causing morphology and structure changes but an increase of cationic order degree in 16d octahedral sites. Li excess could improve the cycle ability by suppressing the Jahn–Teller effect of spinel $LiMn_2O_4$, while Li_2MnO_3 derived from Li-rich for the ternary layered cathodes has a great influence on the electrochemical capability.[20,21] Nevertheless, the impact of lithium excess on $LiNi_{0.5}Mn_{1.5}O_4$ lacks study. Following characterization would provide the result that avoiding the transition metal ion occupation in tetrahedral 8a sites by Li excess is beneficial to the mobility of Li^+. The diffusion channel of Li^+, 8a–16c–8a, is liable to be blocked by transition metal ions in tetrahedral 8a sites, as shown in Fig. 1.

In this work, a one-step nonaqueous co-precipitation method (Fig. S1, ESI†) was applied to precipitate Li^+, Ni^{2+} and Mn^{2+} at the same time to prepare $Li_{1+x}Ni_{0.5-x}Mn_{1.5}O_4$ ($x = 0$, 0.01, 0.03, and 0.05). For the reasonable comparative analysis of these two factors (tetrahedral 8a site occupation and cationic order degree in 16d octahedral sites) influencing the rate performance, keeping identical morphologies for all samples is the prerequisite. It can be found that all the samples display regular, small octahedral grains with a size distribution of 200–500 nm. (Fig. S2, ESI†).

As shown in Fig. 2, the XRD peaks of $LiNi_{0.5}Mn_{1.5}O_4$ and $Li_{1.01}Ni_{0.49}Mn_{1.5}O_4$ coincide well with those of the spinel

[a]Graduate School at Shenzhen, Tsinghua University, Shenzhen 518055, China. E-mail: zhaosx@sz.tsinghua.edu.cn

[b]School of Materials Science and Engineering, Tsinghua University, Beijing 100084, China

[c]Department of Materials Science and Engineering, University of Washington, Seattle, WA 98195, USA

† Electronic supplementary information (ESI) available: Experimental details and other characterization results including SEM, particle size distribution, XPS and rate performance. See DOI: 10.1039/c5ta06339f

Published on 14 September 2015. Downloaded by University of Washington on 19/05/2016 10:25:42.

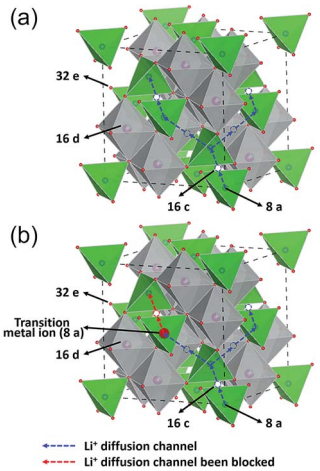

Fig. 1 Schematic illustration of (a) the Li^+ diffusion channel and (b) the Li^+ diffusion channel blocked in the spinel $LiNi_{0.5}Mn_{1.5}O_4$ structure.

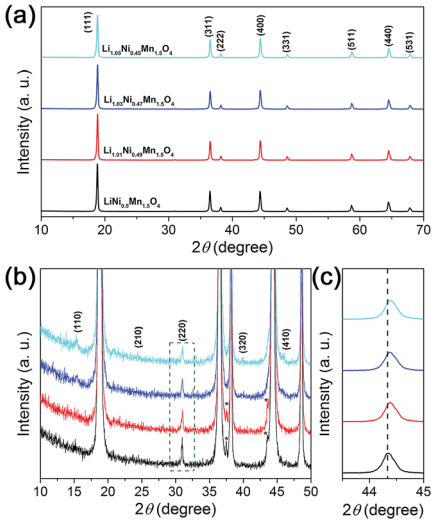

Fig. 2 XRD patterns of the four $Li_{1+x}Ni_{0.5-x}Mn_{1.5}O_4$ samples: (a) full range, (b) enlarged region to show the superstructure reflections arising from the Mn^{4+} and Ni^{2+} ordering in the 16d octahedral sites and (c) enlarged region to show the change of the lattice parameter. Asterisks refer to the reflections arising from the $Li_yNi_{1-y}O$ impurity phase.

structure. The lack of any superstructure diffraction peaks, which derives from the ordering of transition ions in the octahedral 16d sites, reveals that these two samples have a relatively low degree of cationic order.[22] However, increasing the Li amount changes the structure from the disordered to ordered phase, as revealed by the existence of superstructure diffraction peaks such as (110), (210), (320) and (410) peaks.[23] It's worth noting that peaks of the superstructure for $Li_{1.03}Ni_{0.47}Mn_{1.5}O_4$ are weaker than those of $Li_{1.05}Ni_{0.45}Mn_{1.5}O_4$. Of particular note, a diffraction peak appears at $2\theta \approx 30.9°$, which was indexed to the (220) diffraction of the spinel compounds. The appearance of the (220) diffraction peak for $Li_{1+x}Ni_{0.5-x}Mn_{1.5}O_4$ indicates that there must be some transition metal ions occupying the tetrahedral 8a sites replacing the original Li^+ ions.[24] The weak diffraction peaks marked by asterisks possibly are from $Li_yNi_{1-y}O$.[25] This common impurity is only observed in $LiNi_{0.5}Mn_{1.5}O_4$ and $Li_{1.01}Ni_{0.49}Mn_{1.5}O_4$. Arrebola *et al.*[16] considered that based on the crystal field model, in the spinel structure, Ni^{2+} ions have a strong tendency to occupy octahedral 16d positions; therefore Mn was forced to occupy tetrahedral 8a positions. And the radius of Mn^{4+} (0.53 Å) is closer to Li^+ (0.59 Å) than Ni^{2+} (0.69 Å); thus it can be speculated that excess lithium ions could extrude Mn ions out of tetrahedral 8a positions to suppress the formation of Ni-rich impurity.

XPS results show that the Mn valence state in $Li_{1+x}Ni_{0.5-x}Mn_{1.5}O_4$ is between +3 and +4, and the Mn valence state increases with excess Li (Fig. S3, ESI†). The formation of oxygen vacancies could be suppressed by a slow cooling process and then manganese has to take the responsibility to balance charge. In the light of spectral lines of manganese oxide, both the manganese $2p_{3/2}$ and $2p_{1/2}$ regions can be deconvoluted into two peaks. The peaks at 642.0 and 643.3 eV of the $Mn2p_{3/2}$ spectrum arise from Mn^{3+} and Mn^{4+}, respectively, as are those at 653.5 eV for Mn^{3+} and 654.6 eV for Mn^{4+} in the $Mn2p_{1/2}$ spectrum.[26] This can explain the decrease of the lattice parameter of $Li_{1+x}Ni_{0.5-x}Mn_{1.5}O_4$ with Li substitution presented in Fig. 2(c); as we know, Mn^{4+} has a smaller ionic radius ($r = 0.53$ Å) than Mn^{3+} ($r = 0.645$ Å). In a similar manner, Seung M. Oh *et al.*[27] increased the valence state of Mn of $LiMn_2O_4$. The fewer Mn^{3+} ions resulting from Li excess would bring about the higher degree of cationic order, as shown by XRD characterization.

Raman spectroscopy is a helpful testing method to determine the cationic order. According to group theory, the number of expected Raman-active modes of the ordered spinel ($6A_1 + 14E + 22F_2$) is larger than that of the disordered spinel ($A_g + E_g + 3F_{2g}$).[28] Fig. 3(a) shows the Raman spectra of $Li_{1+x}Ni_{0.5-x}Mn_{1.5}O_4$ samples. The peaks at 640 cm^{-1} (symmetric Mn–O stretching vibration of MnO_6 groups) result from the A_g mode, and the lines at 498 and 402 cm^{-1} can be assigned to the Ni^{2+}–O stretching mode in the structure. The increasing intensity of

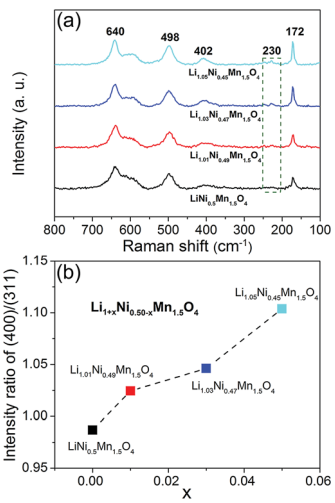

Fig. 3 (a) Raman spectra of $Li_{1+x}Ni_{0.5-x}Mn_{1.5}O_4$ samples, and (b) the intensity ratio of (400)/(311) XRD peaks.

This journal is © The Royal Society of Chemistry 2015

Published on 14 September 2015. Downloaded by University of Washington on 19/05/2016 10:25:42.

peaks at 172 and 230 cm^{-1} is characteristic of a more ordered structure.[13] It can be found that as the amount of lithium increases, the degree of cationic ordering increases, which is in accordance with XRD results. Besides, many researchers[12,15,17,24] used the intensity ratio of (400)/(311) of the XRD pattern to estimate the distribution of transition metal ions between the 8a sites and 16d sites in the spinel structure. As shown in Fig. 3(b), the intensity ratio of (400)/(311) increases as the amount of lithium increases, indicating that the amount of transition metal ions in tetrahedral 8a sites is reduced by excess lithium ions.

The high resolution electron microscopy images are compared in Fig. 4 along with the diffraction patterns in the [100] and [110] zones. Fig. 4(a1)–(d1) show the HRTEM images of the lattice fringe, in which d_{hkl} measured is ~0.47 nm, corresponding to the (111) interplanar distance. Only a representative spinel diffraction pattern can be observed in the [100] and [110] zones for $Li_{1+x}Ni_{0.5-x}Mn_{1.5}O_4$ ($x = 0$, 0.01, and 0.03), while $Li_{1.05}Ni_{0.45}Mn_{1.5}O_4$ exhibits superlattice diffraction as shown in Fig. 4(d2 and d3).[29] The electron diffraction patterns show that the increasing Li amount introduces a more ordered phase (or decreases disordered phase) content as well.

Galvanostatic cycling tests were conducted at a current density of 14.7 mA g^{-1} (0.1C) from 3.5 to 5.0 V, as shown in Fig. 5(a). All the cathodes exhibited two typical plateaus: a long and distinct flat plateau around 4.7 V attributed to the $Ni^{2+/4+}$ redox reaction, and another short plateau around 4.0 V arising from the $Mn^{3+/4+}$ redox process.[30] The voltage plateau of 4.0 V indicates that a small amount of manganese remained as Mn^{3+},[31] because the oxidation state of manganese is fixed at +4 only in the ideal structure.[29] The length fraction of the plateau at 4.0 V decreases by increasing the Li fraction. This trend can be accounted for by considering that an increase in Li amount results in a decrease of the Mn^{3+} concentration, in accordance with XRD, XPS and TEM results. Besides, it is worth noting that the charge plateau of $LiNi_{0.5}Mn_{1.5}O_4$ and $Li_{1.01}Ni_{0.49}Mn_{1.5}O_4$ samples around 4.7 V splits into two plateaus corresponding to

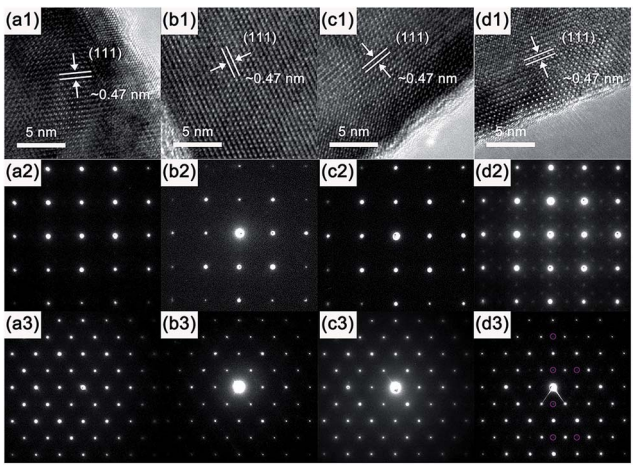

Fig. 4 HRTEM images (a1 to d1) and electron diffraction patterns in the [100] (a2 to d2) and [110] (a3 to d3) zones of (a) $LiNi_{0.5}Mn_{1.5}O_4$, (b) $Li_{1.01}Ni_{0.49}Mn_{1.5}O_4$, (c) $Li_{1.03}Ni_{0.47}Mn_{1.5}O_4$ and (d) $Li_{1.05}Ni_{0.45}Mn_{1.5}O_4$.

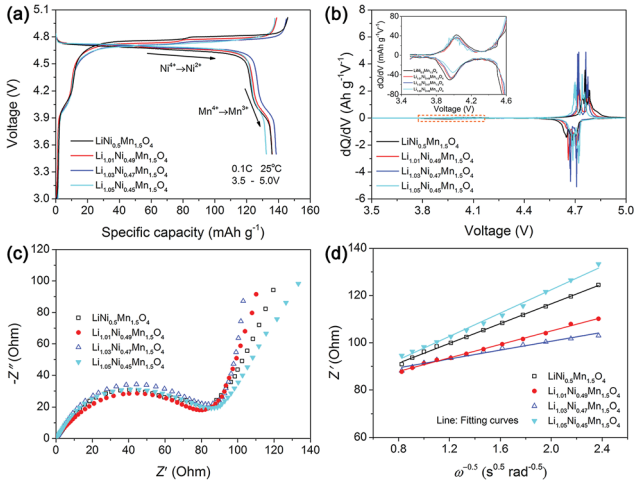

Fig. 5 (a) Charge and discharge profiles, (b) dQ/dV *versus* voltage in the 4 V region, (c) EIS spectra at 25 °C before cycling and (d) Z_{re} *vs.* $\omega^{-0.5}$ plots in the low-frequency region obtained from EIS measurements of the four $Li_{1+x}Ni_{0.5-x}Mn_{1.5}O_4$ samples.

$Ni^{4+/3+}$ and $Ni^{3+/2+}$ couples individually as shown in Fig. 5(a), while these two plateaus overlapped for $Li_{1.03}Ni_{0.47}Mn_{1.5}O_4$ and $Li_{1.05}Ni_{0.45}Mn_{1.5}O_4$. It has been reported that the narrower separation between the two voltage plateaus indicates a higher degree of cationic ordering.[32] A more detailed analysis is further possible with the dQ/dV plots (Q = specific capacity and V = voltage). The two dQ/dV peaks in the 4.7 V region indicate, respectively, the two-step oxidation or reduction for the $Ni^{4+/2+}$ redox couple. The inset of Fig. 5(b) is the dQ/dV plots in the 4 V region of the spinel cathodes, also showing that the intensity of the peak in the 4.0 V region reduces by increasing the Li fraction.

In order to study the effect of excess lithium on diffusion of Li^+ in the cathodes, electrochemical impedance spectroscopy was performed. Fig. 5(c) displays the Nyquist plots of the spinel electrodes before cycling. All EIS spectra contain one semicircle in the high- and medium-frequency regions and an inclined line in the low frequency zone. The diffusion coefficient (D_{Li}) of lithium ions can be calculated from the plots in the low-frequency region using the equation:[33]

$$D_{Li} = \frac{(RT)^2}{2(An^2F^2C_{Li}\sigma)^2}$$

where T is the kelvin degree, R is the universal gas constant, n is the number of electrons per molecule during the reaction, A is the superficial area, F is Faraday's constant, C_{Li} is the lithium ion concentration, ω is the angular frequency, and σ is the Warburg factor. The Z_{re}–$\omega^{-0.5}$ plots to calculate σ are presented in Fig. 5(d). A linear characteristic could be seen for both profiles. The calculated lithium ion diffusion coefficient of $Li_{1.03}Ni_{0.47}Mn_{1.5}O_4$ is higher than that of the other three samples, which is calculated to be 3.159×10^{-10} cm^2 s^{-1} and close to that measured by CV.[34] Interestingly, though $Li_{1.03}Ni_{0.47}Mn_{1.5}O_4$ exhibits a higher degree of cationic ordering than $LiNi_{0.5}Mn_{1.5}O_4$ and $Li_{1.01}Ni_{0.49}Mn_{1.5}O_4$, it exhibits better

Published on 14 September 2015. Downloaded by University of Washington on 19/05/2016 10:25:42.

lithium ion diffusion capability, implying that the well-known factor, cationic order degree in 16d octahedral sites, does not dominate the Li^+ transport for these three samples.

The cycle and rate performances (Fig. 6) are in good agreement with EIS results. At 25 °C, the $LiNi_{0.5}Mn_{1.5}O_4$, $Li_{1.01}Ni_{0.49}Mn_{1.5}O_4$, $Li_{1.03}Ni_{0.47}Mn_{1.5}O_4$ and $Li_{1.05}Ni_{0.45}Mn_{1.5}O_4$ samples delivered initial specific capacities of 105.9, 114.8, 123.7 and 88.1 mA h g^{-1} at a 5C rate and retained 93.4%, 95.0%, 95.7% and 96.0% after 300 cycles, respectively. It can be seen that the coulombic efficiency of the initial cycle for all the samples is relatively low because the batteries were charged at 0.1C, and then discharged at 5C, but it became higher and stable in the following cycles. The Li-excess samples exhibited higher coulombic efficiency resulting in better cycle performance. The cycle ability is comparable with that of $LiNi_{0.5}Mn_{1.5}O_4$ nanotubes synthesized by a self-templating method, which delivered a discharge capacity of 85 mA h g^{-1} at 5C even after 550 cycles.[35] At a high rate of 30C, the discharge capacity of $Li_{1.03}Ni_{0.47}Mn_{1.5}O_4$ can still reach 90.1 mA h g^{-1}, corresponding to 72.8% of its capacity at 1C. It is important to note that the discharge specific capacity at high C-rates was significantly improved for $Li_{1.03}Ni_{0.47}Mn_{1.5}O_4$ compared with other samples. The $Li_{1.03}Ni_{0.47}Mn_{1.5}O_4$ electrode displays a discharge capacity of 114.2 mA h g^{-1} at 10C-rate. In contrast, the rate behaviour of $Li_{1.05}Ni_{0.45}Mn_{1.5}O_4$ worsens dramatically; it presents a discharge capacity of only 87.3 mA h g^{-1} when the current density increases to 10C.

Many researchers have reported that a high degree of cationic ordering would deteriorate the rate performance due to limited lithium diffusion.[36] In this study, the $Li_{1.05}Ni_{0.45}Mn_{1.5}O_4$ electrode with the highest order degree indeed shows the worst rate capability. By comparing the rate ability of $Li_{1.03}Ni_{0.47}Mn_{1.5}O_4$ to $Li_{1.05}Ni_{0.45}Mn_{1.5}O_4$, it can be found that $Li_{1.05}Ni_{0.45}Mn_{1.5}O_4$ with a higher degree of cationic ordering delivers lower rate ability. This could be because the degree of cationic ordering plays a leading role for these two samples, in agreement with the general view.[37] However, for the first three samples ($LiNi_{0.5}Mn_{1.5}O_4$, $Li_{1.01}Ni_{0.49}Mn_{1.5}O_4$, and $Li_{1.03}Ni_{0.47}Mn_{1.5}O_4$), excess lithium improved the rate ability obviously, indicating that the transport of lithium ions could be enhanced by an unhindered diffusion channel even with a more ordered arrangement of nickel and manganese ions in 16d octahedral sites.

In conclusion, octahedral grains of $LiNi_{0.5}Mn_{1.5}O_4$-based materials are synthesized through a one-step co-precipitation method. A series of samples with increasing degree of cationic ordering in 16d octahedral sites (harmful to mobility of Li^+) were prepared, in which the amount of transition metal ions in tetrahedral 8a sites reduces (beneficial for Li^+ diffusion). The improved performance of $Li_{1.03}Ni_{0.47}Mn_{1.5}O_4$ might be attributed to appropriate excess lithium ions which can preferentially occupy the tetrahedral 8a sites, extruding transition metal ions out of tetrahedral 8a positions to keep the Li^+ ion diffusion channel unobstructed. However, when the lithium excess is too much, it will result in obvious enhancement of the order degree in octahedral 16d sites, which is widely accepted as a negative factor for rate capacity.

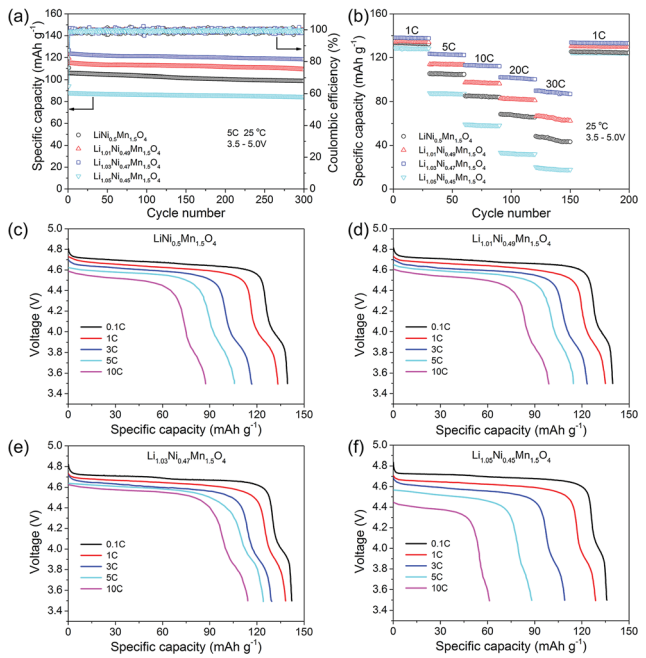

Fig. 6 Cycling stability of $Li_{1+x}Ni_{0.5-x}Mn_{1.5}O_4$ electrodes at (a) 5C rate and (b) various rates (1C, 5C, 10C, 20C, and 30C); discharge profiles of (c) $LiNi_{0.5}Mn_{1.5}O_4$, (d) $Li_{1.01}Ni_{0.49}Mn_{1.5}O_4$, (e) $Li_{1.03}Ni_{0.47}Mn_{1.5}O_4$ and (f) $Li_{1.05}Ni_{0.45}Mn_{1.5}O_4$.

Acknowledgements

This work was supported by the National Natural Science Foundation of China (51172124, 51372136) and Shenzhen Basic Research Project (No. JCYJ20130402145002372).

Notes and references

1 P. Y. Hou, J. Wang, J. S. Song, D. W. Song, X. X. Shi, X. Q. Wang and L. Q. Zhang, *Chem. Commun.*, 2015, **51**, 3231–3234.
2 R. R. Liu, X. Deng, X. R. Liu, H. J. Yan, A. M. Cao and D. Wang, *Chem. Commun.*, 2014, **50**, 15756–15759.
3 K. Zhang, X. P. Han, Z. Hu, X. L. Zhang, Z. L. Tao and J. Chen, *Chem. Soc. Rev.*, 2015, **44**, 699–728.
4 E. S. Lee, K. W. Nam, E. Y. Hu and A. Manthiram, *Chem. Mater.*, 2012, **24**, 3610–3620.
5 K. M. Shaju and P. G. Bruce, *Dalton Trans.*, 2008, 5471–5475.
6 K. R. Chemelewski, D. W. Shin, W. Li and A. Manthiram, *J. Mater. Chem. A*, 2013, **1**, 3347–3354.
7 B. Hai, A. K. Shukla, H. Duncan and G. Y. Chen, *J. Mater. Chem. A*, 2013, **1**, 759–769.
8 H. F. Deng, P. Nie, L. F. Shen, H. F. Luo and X. G. Zhang, *Progr. Chem.*, 2014, **26**, 939–949.
9 L. P. Wang, H. Li, X. J. Huang and E. Baudrin, *Solid State Ionics*, 2011, **193**, 32–38.
10 J. Xiao, X. L. Chen, P. V. Sushko, M. L. Sushko, L. Kovarik, J. J. Feng, Z. Q. Deng, J. M. Zheng, G. L. Graff, Z. M. Nie,

 This journal is © The Royal Society of Chemistry 2015

Published on 14 September 2015. Downloaded by University of Washington on 19/05/2016 10:25:42.

D. W. Choi, J. Liu, J. G. Zhang and M. S. Whittingham, *Adv. Mater.*, 2012, **24**, 2109–2116.
11 J. Song, D. W. Shin, Y. H. Lu, C. D. Amos, A. Manthiram and J. B. Goodenough, *Chem. Mater.*, 2012, **24**, 3101–3109.
12 H. L. Wang, T. A. Tan, P. Yang, M. O. Lai and L. Lui, *J. Phys. Chem. C*, 2011, **115**, 6102–6110.
13 X. L. Zhang, F. Y. Cheng, K. Zhang, Y. L. Liang, S. Q. Yang, J. Liang and J. Chen, *RSC Adv.*, 2012, **2**, 5669–5675.
14 K. Amine, H. Tukamoto, H. Yasuda and Y. Fujita, *J. Power Sources*, 1997, **68**, 604–608.
15 T. Ohzuku, K. Ariyoshi, S. Takeda and Y. Sakai, *Electrochim. Acta*, 2001, **46**, 2327–2336.
16 J. C. Arrebola, A. Caballero, M. Cruz, L. Hernan, J. Morales and E. R. Castellon, *Adv. Funct. Mater.*, 2006, **16**, 1904–1912.
17 T. F. Yi, C. Y. Li, Y. R. Zhu, J. Shu and R. S. Zhu, *J. Solid State Electrochem.*, 2009, **13**, 913–919.
18 H. L. Wang, H. Xia, M. O. Lai and L. Lu, *Electrochem. Commun.*, 2009, **11**, 1539–1542.
19 Y. Cho, S. Lee, Y. Lee, T. Hong and J. Cho, *Adv. Energy Mater.*, 2011, **1**, 821–828.
20 S. Taminato, M. Hirayama, K. Suzuki, N. L. Yamada, M. Yonemura, J. Y. Son and R. Kanno, *Chem. Commun.*, 2015, **51**, 1673–1676.
21 S. Komaba, N. Kumagai, T. Sasaki and Y. Miki, *Electrochemistry*, 2001, **69**, 784–787.
22 F. G. B. Ooms, E. M. Kelder, J. Schoonman, M. Wagemaker and F. M. Mulder, *Solid State Ionics*, 2002, **152**, 143–153.
23 M. Kunduraci and G. G. Amatucci, *J. Electrochem. Soc.*, 2006, **153**, A1345–A1352.
24 Y. S. Lee, Y. K. Sun and K. S. Nahm, *Solid State Ionics*, 1998, **109**, 285–294.
25 H. F. Luo, P. Nie, L. F. Shen, H. S. Li, H. F. Deng, Y. Y. Zhu and X. G. Zhang, *ChemElectroChem*, 2015, **2**, 127–133.
26 X. G. Hao, M. H. Austin and B. M. Bartlett, *Dalton Trans.*, 2012, **41**, 8067–8076.
27 J. H. Lee, J. K. Hong, D. H. Jang, Y. K. Sun and S. M. Oh, *J. Power Sources*, 2000, **89**, 7–14.
28 N. Amdouni, K. Zaghib, F. Gendron, A. Mauger and C. M. Julien, *Ionics*, 2006, **12**, 117–126.
29 J. H. Kim, S. T. Myung, C. S. Yoon, S. G. Kang and Y. K. Sun, *Chem. Mater.*, 2004, **16**, 906–914.
30 Q. M. Zhong, A. Bonakdarpour, M. J. Zhang, Y. Gao and J. R. Dahn, *J. Electrochem. Soc.*, 1997, **144**, 205–213.
31 J. H. Cho, J. H. Park, M. H. Lee, H. K. Song and S. Y. Lee, *Energy Environ. Sci.*, 2012, **5**, 7124–7131.
32 D. W. Shin, C. A. Bridges, A. Huq, M. P. Paranthaman and A. Manthiram, *Chem. Mater.*, 2012, **24**, 3720–3731.
33 A. Y. Shenouda and H. K. Liu, *J. Power Sources*, 2008, **185**, 1386–1391.
34 X. Fang, N. Ding, X. Y. Feng, Y. Lu and C. H. Chen, *Electrochim. Acta*, 2009, **54**, 7471–7475.
35 G. Q. Wang, J. Xie, T. J. Zhu, G. S. Cao, X. B. Zhao and S. C. Zhang, *Funct. Mater. Lett.*, 2014, **7**, 1450009.
36 A. Manthiram, K. Chemelewski and E. S. Lee, *Energy Environ. Sci.*, 2014, **7**, 1339–1350.
37 K. R. Chemelewski and A. Manthiram, *J. Phys. Chem. C*, 2013, **117**, 12465–12471.